⌘ *Author's Choice*

THE JOURNAL OF BIOLOGICAL CHEMISTRY VOL. 285, NO. 22, pp. 17137–17147, May 28, 2010

Stacked Sets of Parallel, In-register β-Strands of β_2-Microglobulin in Amyloid Fibrils Revealed by Site-directed Spin Labeling and Chemical Labeling*

Received for publication, February 23, 2010, and in revised form, March 23, 2010 Published, JBC Papers in Press, March 24, 2010, DOI 10.1074/jbc.M110.117234

Carol L. Ladner[‡1], Min Chen[§1], David P. Smith[‡2], Geoffrey W. Platt[‡], Sheena E. Radford[‡3], and Ralf Langen[§4]

From the [‡]Astbury Centre for Structural Molecular Biology, University of Leeds, Leeds LS2 9JT, United Kingdom and the [§]Zilkha Neurogenetic Institute, Keck School of Medicine, University of Southern California, Los Angeles, California 90033

β_2-microglobulin (β_2m) is a 99-residue protein with an immunoglobulin fold that forms β-sheet-rich amyloid fibrils in dialysis-related amyloidosis. Here the environment and accessibility of side chains within amyloid fibrils formed *in vitro* from β_2m with a long straight morphology are probed by site-directed spin labeling and accessibility to modification with *N*-ethyl maleimide using 19 site-specific cysteine variants. Continuous wave electron paramagnetic resonance spectroscopy of these fibrils reveals a core predominantly organized in a parallel, in-register arrangement, by contrast with other β_2m aggregates. A continuous array of parallel, in-register β-strands involving most of the polypeptide sequence is inconsistent with the cryo-electron microscopy structure, which reveals an architecture based on subunit repeats. To reconcile these data, the number of spins in close proximity required to give rise to spin exchange was determined. Systematic studies of a model protein system indicated that juxtaposition of four spin labels is sufficient to generate exchange narrowing. Combined with information about side-chain mobility and accessibility, we propose that the amyloid fibrils of β_2m consist of about six β_2m monomers organized in stacks with a parallel, in-register array. The results suggest an organization more complex than the accordion-like β-sandwich structure commonly proposed for amyloid fibrils.

Dialysis-related amyloidosis is a debilitating disorder in which β_2m[5] deposits in amyloid fibrils within cartilage-rich joints, resulting in carpal tunnel syndrome and pathological bone destruction (1). β_2m is a 99-residue protein that adopts a β-sandwich fold, where the two β-sheets are formed entirely from anti-parallel β-strands linked by an intersheet disulfide bond (2). *In vitro* β_2m forms two different types of fibrils, through competing pathways (3). Long straight fibrils, which possess all the hallmarks of amyloid, form at acidic pH and low ionic strength, through a nucleation-dependent mechanism (4, 5). By contrast, wormlike fibrils form at acidic pH and high salt concentrations with lag phase-independent kinetics (3, 5, 6) (Fig. 1*A*). These wormlike assemblies give rise to some of the characteristic signatures of amyloid, with weak thioflavin T fluorescence and the ability to bind Congo red, but they show weak binding to amyloid-specific antibodies and produce fiber diffraction patterns consistent with less organized fibril types (5, 7).

The structural properties of long straight β_2m fibrils generated at acidic pH have been investigated by limited proteolysis (8, 9) and hydrogen/deuterium exchange experiments (10, 11), but despite this, there is no atomic molecular model for the fibril structure. Hydrogen/deuterium exchange NMR indicates a hydrogen-bonded core stretching from residue 21 to 85, with the N-terminal and C-terminal regions showing weaker protection from exchange (10, 11). Limited proteolysis suggests a core region composed of residues 9–96 or 20–87, dependent on the protease used (8, 9). By contrast with these results, recent ^{1}H NMR experiments showed that the entire sequence of β_2m, including the N- and C-terminal residues, to be immobile in the fibril structure, with ^{15}N/^{1}H signals being observed only when the N terminus was extended by a $(Gly\text{-}Ser\text{-}Gly)_3$ sequence (12). FTIR spectroscopy shows an ordered β-sheet structure for the long straight fibrils of β_2m, with a maximum absorbance at 1620 cm^{-1} typical of amyloid (13–15). Recent analysis of the fibril three-dimensional structure using cryo-EM revealed a complex organization involving an array of subunits stacked in repeats that are 5.2–6.5 nm in height (16). These data, combined with information obtained from proline-scanning (17) and tryptophan-scanning mutagenesis (18), suggest a complex architecture for β_2m fibrils in which the polypeptide chain must adopt a highly non-native conformation that nonetheless retains the native disulfide cross-link between residues 25 and 80 (19). Although this information provides an indication of the general protein conformation of β_2m in the fibrils, it does not explain how β_2m is arranged in the structure previously revealed by cryo-EM.

In the present study, the organization of the polypeptide chain of β_2m and the side-chain dynamics and accessibility within long straight fibrils are determined. For this purpose, variants containing a newly introduced cysteine residue were created for site-directed spin labeling, and continuous wave

* This work was supported, in whole or in part, by National Institutes of Health Grant AG027936. This work was also supported by Wellcome Trust Grants 080859/B/06/Z, GR075675MA, and WT069851MA and the Hillblom Foundation.

⌘ *Author's Choice*—Final version full access.

[1] Both authors contributed equally to this work.

[2] Present address: Biomedical Research Centre, Sheffield Hallam University, Sheffield S1 1WB, United Kingdom.

[3] To whom correspondence may be addressed. Tel.: 44-113-343-3170; Fax: 44-113-343-7486; E-mail: s.e.radford@leeds.ac.uk.

[4] To whom correspondence may be addressed. Tel.: 323-442-1323; Fax: 323-442-4404; E-mail: langen@usc.edu.

[5] The abbreviations used are: β_2m, β_2-microglobulin; FTIR, Fourier transform infrared; NEM, *N*-ethylmaleimide; MTSL, 1-oxyl-2,2,5,5-tetramethyl-D-pyrroline-3-methyl-methanethiosulfonate label; ESI, electrospray ionization; MS, mass spectrometry; DTT, dithiothreitol.

electron paramagnetic resonance was used to elucidate the organization and mobility of the spin-labeled positions. Side-chain accessibility was also determined by assessing the reactivity of the introduced thiol to labeling with *N*-ethylmaleimide (NEM). By comparison with analysis of the monomer in isolation and within wormlike fibrils, the results reveal that the core of long straight fibrils contains a parallel in-register structure. In order to reconcile this information with the discontinuous densities observed by cryo-EM, we determined how many spin labels are required to be in close contact to give rise to spin exchange narrowing in EPR spectra. Using amphiphysin as a model protein, we report here that four spin labels give rise to exchange narrowing provided that the labels are in close contact (<7 Å). Together, these data provide a model for long straight fibrils of β_2m in which the subunit repeat revealed by cryo-EM consists of stacks of approximately six β-strands organized in a parallel, in-register structure.

EXPERIMENTAL PROCEDURES

Site-directed Mutagenesis and Protein Purification—Plasmids encoding genes for the single cysteine mutants of β_2m were created by PCR mutagenesis of the pINK plasmid containing the human β_2m gene in pET23a (20) using QuikChange site-directed mutagenesis (Stratagene). Clones of the single cysteine mutants, with confirmed sequence, were expressed in *Escherichia coli* strain BL21(DE3) pLysS as inclusion bodies. β_2m was purified as described previously (6). For some cysteine mutants, refolding from urea into buffer was optimized by the inclusion of various combinations of 0 or 2 mM reduced glutathione; 0, 0.2, or 0.4 mM oxidized glutathione; 0 or 0.64 M arginine; and 0 or 20 mM NaCl (21). In each case, the protein in 8 M urea was diluted to ~5 mg/ml in the optimized buffer and dialyzed into 2–5 liters of the selected buffer. Further dialysis was performed in 20 mM Tris-HCl, pH 8, or 20 mM Tris-HCl, pH 8, containing 20 mM NaCl.

Refolded protein was purified by anionic exchange with Q-Sepharose fast flow resin (GE Healthcare) as described previously (6). To refolded cysteine mutants, 5 mM dithiothreitol (DTT) was added before loading onto the Q-Sepharose column, and protein was eluted with a 0–1 M NaCl gradient in 20 mM Tris-HCl, pH 8. β_2m was then dialyzed into 18-megaohm water or 20 mM NH_4HCO_3 for lyophilization. This lyophilized protein was further purified by gel filtration following resuspension in 20 mM Tris-HCl, pH 8, containing 5 mM DTT and gel filtration in the same buffer, but lacking DTT, using a Superdex 75 HiLoad column. Protein was lyophilized and stored at −20 °C. For wild-type β_2m, a yield of 30 mg of pure protein/liter of culture was obtained. For cysteine mutants, the yield ranged from 0.5 to 10 mg of pure protein/liter. All proteins were pure by SDS-PAGE, and the molecular weight was confirmed by ESI-MS.

Spin Labeling β_2m—Purified single cysteine mutants were spin-labeled with 1-oxyl-2,2,5,5-tetramethyl-D-pyrroline-3-methyl-methanethiosulfonate (MTSL) (Toronto Research Chemicals, Canada) in a manner similar to that described previously (22). β_2m cysteine mutants were dissolved in 25 mM Tris-HCl, pH 8, 5 mM DTT, 1 mM EDTA and incubated at room temperature for 20 min. This step reduces intermolecular disulfide bonds while leaving the intrachain disulfide bond intact (23). The DTT was then removed on a Nap-10 column (Sephadex G-25, GE Healthcare), and the protein was immediately spin-labeled. Spin labeling was conducted in 25 mM sodium phosphate buffer, pH 7, containing 1 mM EDTA and 2.4 M guanidinium HCl with a 10-fold molar excess of MTSL at room temperature for 2 h with rocking. The labeled protein was then purified from unreacted MTSL on a PD-10 column (Sephadex G-25, GE Healthcare), and singly spin-labeled β_2m was purified from unlabeled protein on a Resource Q ion exchange column (GE Healthcare). The resulting protein was buffer-exchanged into 18-megaohm water using a Centricon concentrator (molecular weight cut-off 3,000) and stored at −20 °C. 100% pure spin-labeled β_2m was confirmed by ESI-MS. Non-reducing SDS-PAGE of labeled β_2m showed a migration similar to that of the wild-type protein, confirming the absence of disulfide-bonded dimers. The position of the spin label was confirmed by peptide mapping mass spectrometry (not shown).

Fibril Formation—For growth of long straight fibrils, β_2m was first prepared by dissolving the lyophilized protein in either water, 3 mM HCl, or 25 mM sodium phosphate buffer, pH 7, and filtered using a 0.22-μm MiniSart fast flow filter (Sartorius Stedim Biotech). The protein was then diluted to 0.5 mg/ml β_2m in 25 mM sodium phosphate buffer, pH 2.5. Fibrillar seeds formed from the wild-type protein at pH 2.5 (5% (w/w) seeds) were then added, and fibril growth was continued by shaking the sample at 200 rpm for 3–12 days at 37 °C (20). Spin-labeled fibrils were grown from 10, 25, 50, 75, or 100% MTSL-labeled monomers by mixing the appropriate amount of spin labeled β_2m with wild-type β_2m. Wormlike fibrils were prepared with protein at 1.0 mg/ml in 25 mM sodium phosphate buffer, pH 2.5, 400 mM NaCl grown quiescently at 37 °C, as described previously (3).

Negative Stain EM—Fibrils assembled as described above were diluted 3–10-fold in 3 mM HCl and placed on glow-discharged colloidion-coated copper grids and stained with 4% (w/v) uranyl acetate. Images were taken on a Philips CM10 electron microscope operating at 80 keV.

FTIR—Transmission mode FTIR spectra were acquired of different samples prepared from wild-type, spin-labeled, or unlabeled cysteine mutants of β_2m. Fibrils for FTIR were made from D_2O-exchanged protein (exchanged overnight from lyophilized protein, pD 5, in D_2O at room temperature and filtered). Fibrils were formed as described above, except that all buffers were prepared in D_2O. Long straight fibrils were then centrifuged for 10 min at 13,000 × *g*, wormlike fibrils were centrifuged for 2 h at 16,300 × *g*, and the resulting pellets were resuspended in D_2O/DCl, pD 2.1. Samples of 0.5–1 mg of protein in 50 μl were loaded between CaF_2 plates with a 0.05-mm Teflon spacer. Spectra were acquired from 256 integrated scans with an aperture of 32 and resolution of 4 cm^{-1} at room temperature on a Thermo-Nicolet 560 FTIR spectrometer with a mercury-cadmium-telluride detector purged with dry air. For each sample, a buffer spectrum was subtracted, and residual water vapor peaks were removed. Spectra were smoothed with Savitzky-Golay 9-point smoothing, and second derivatives were obtained in OMNIC ESP 5.0 software.

Limited Proteolysis of Fibrils—The fibril core protected from proteolysis was investigated by limited pepsin digestion as

described previously (9). Briefly, fibrils were digested by resuspending pelleted fibrils in 25 mM sodium phosphate buffer, pH 2.5, containing pepsin (Sigma) at a 1:100 (w/w) pepsin/β_2m ratio. Samples were removed at intervals of 1 min, 10 min, 15 min, and 1 h, and proteolysis was inhibited by the addition of 5 μM pepstatin. The digested fibrils were then pelleted by centrifugation at 13,000 × *g* for 30 min, the pellet was washed with water, and fibrils were subsequently dissolved in 100% hexafluoroisopropanol and air-dried. ESI mass spectra were then acquired for each sample on an LCT-Premier mass spectrometer (Waters UK Ltd., Manchester, UK) with a NanoMate (Advion, Ithaca, NY) autosampler and nano-ESI interface.

Expression, Purification, and Spin Labeling of Amphiphysin—Variants of His_6-tagged *Drosophila melanogaster* amphiphysin, engineered with single site cysteines introduced into a sequence in which the two native cysteines were replaced with alanines, was expressed using a pET expression vector in *E. coli* BL21(DE3) pLysS cells. Expression was induced at 14 °C overnight, and cells were lysed in resuspension buffer containing 20 mM HEPES, pH 7.0, 500 mM NaCl, 1 mM DTT, and 1 mM EDTA. Cell lysate, prepared by sonication, was clarified by centrifugation, and the amphiphysin was purified on a HiTrap HP Ni^{2+}-nitrilotriacetic acid column (GE Healthcare). Concentrated protein was then applied to a Superdex 200 gel filtration column equilibrated in the resuspension buffer, followed by ion exchange on a Mono-S HR5/5 column (GE Healthcare) eluted with a 0–2 M NaCl gradient in 20 mM HEPES, pH 7.0, 1 mM DTT, and 1 mM EDTA. Protein was shown to be pure by SDS-PAGE, and the concentration was determined by a Micro BCA protein assay kit (Pierce). Immediately before spin labeling, DTT was removed using a PD-10 column (GE Healthcare) using buffer containing 20 mM HEPES, pH 7.0, 500 mM NaCl, and 1 mM EDTA. Amphiphysin was labeled with a 10-fold molar excess of MTSL for 1 h at room temperature, and excess label was removed using PD-10 columns.

X-band EPR Spectroscopy and Data Analysis—The derivatized β_2m fibrils and monomers as well as amphiphysin were loaded into quartz capillaries (0.6-mm inner diameter × 0.84-mm outer diameter, VitroCom, Mt. Lakes, NJ), and EPR spectra were acquired on X-band Bruker EMX spectrometers (Bruker Instruments, Billerica, MA). Sucrose was added to monomer to reduce tumbling of the protein so that the line shape is influenced by label motion rather than protein tumbling.

Full spectral scans were obtained using an ER 4119HS resonator at room temperature. The spectral scans performed at room temperature using the ER 4119HS resonator were swept for a 150 gauss scan width at an incident microwave power of 12 milliwatts.

NEM Labeling of Monomer and Fibrils—Monomer and fibrils were labeled with a 100-fold molar excess of NEM (Pierce) over the β_2m concentration for 10 min at room temperature, in 25 mM sodium phosphate buffer, pH 7, containing 84 μM Tris(2-carboxyethyl)phosphine HCl (Pierce). To label fibrils, 400 μl of the fibril growth mixture at pH 2.5 was brought to pH 7 with NaOH. Immediately after increasing the pH, NEM was added, and, after 10 min of occasional mixing, the reaction was quenched with DTT (at a 20-fold molar excess relative to the concentration of NEM), and the pH was decreased to pH 2.1–2.5 with HCl. After labeling, the fibrils were centrifuged for 10 min at 16,300 × *g*, and the pellet was washed by repeated suspension (three times) in 50 mM ammonium formate, pH 2.5, and recentrifugation. This fibril pellet was then suspended in 50 μl of hexafluoroisopropanol and shaken for 2–12 h at 37 °C to dissolve the fibrils. The sample was then air-dried and dissolved in 5 μl of hexafluoroisopropanol, 10 μl of 50% methanol, and 1 mM Tris(2-carboxyethyl)phosphine HCl for analysis by ESI-MS. Monomer was labeled at a concentration of 0.5 mg/ml in 25 mM sodium phosphate buffer, pH 7, with a 100-fold molar excess of NEM, containing 84 μM Tris(2-carboxyethyl)phosphine HCl, and the reaction was quenched after 10 min as described above. The sample was then immediately precipitated by the addition of 9 volumes of acetone at −20 °C for 1 h, and the precipitate was collected by centrifugation at 16,300 × *g* for 5 min at 4 °C. The pellet was washed with 1 ml of 90% ethanol at −20 °C, air-dried and dissolved in 10 μl of hexafluoroisopropanol, 20 μl of 50% methanol, and 1 mM Tris(2-carboxyethyl)phosphine HCl for analysis by ESI-MS.

The reaction time and conditions were chosen to allow the reaction to proceed to completion for the R3C variant monomer. Various controls were performed in developing the NEM labeling protocol to ensure that labeling was specific to the single newly introduced cysteine. First, no NEM labeling of wild-type β_2m in the monomeric or fibrillar state occurred under the conditions used. Second, negative stain EM and thioflavin T fluorescence showed that the fibrils remained intact during the labeling conditions, and monomer dissociation (and thereby its labeling) under the conditions employed was <10%. Furthermore, labeling within the fibrils rather than only at the fibril ends (wherein monomer dissociation is maximal) was demonstrated by extending fibrils formed from cysteine mutants with ^{15}N-labeled wild-type β_2m monomers (12) and determining the extent of labeling of the single cysteine variant. Within the error of these measurements, the percentage labeling was identical to that of fibrils that had not been extended with wild-type monomer (data not shown).

Quantitation of the Extent of NEM Labeling—ESI mass spectra were acquired on a LCT-Premier mass spectrometer. Samples prepared as described above were diluted 5-fold into 50% methanol, 0.1% formic acid and then ionized and desolvated at a capillary voltage of 1.5 kV, with nitrogen as nebulizing gas at 0.3 p.s.i., cone voltage at 70 V, and source temperature at 60 °C. A mass range of 500–3000 m/z was collected. Spectra were externally calibrated with horse heart myoglobin. Peaks were integrated using the area of peaks from three charge states in MassLynx (Waters UK Ltd.). The unlabeled and NEM-labeled peaks were integrated and used as a quantitative measure of the percentage labeling at each site. NEM reactivity was calculated as the ratio of NEM-labeled product as follows,

$$\%\ \text{NEM label} = (I_{\text{labeled}})/(I_{\text{labeled}} + I_{\text{unlabeled}}{}^{*}) \times 100 \quad \text{(Eq. 1)}$$

where $I_{\text{unlabeled}}{}^{*} = I_{\text{unlabeled}} \times f_m$. The fraction of monomeric protein (f_m), was determined from non-reducing SDS-PAGE with samples treated with iodoacetamide and was used to correct for any residual disulfide-bonded dimers in the labeling reaction.

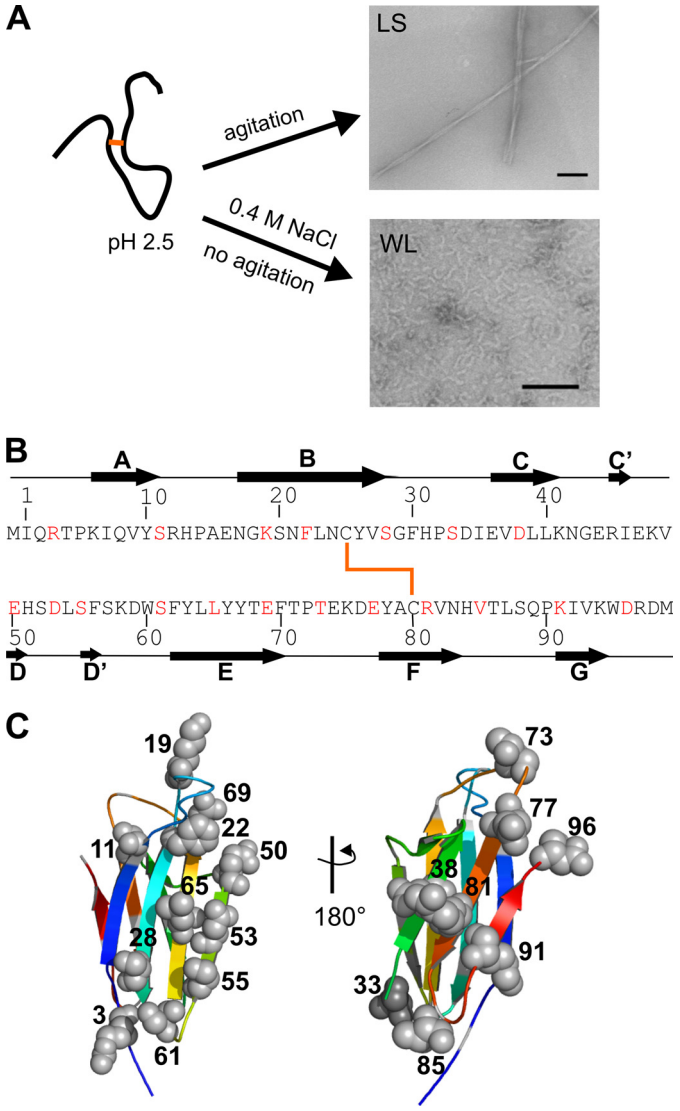

FIGURE 1. **Single cysteine mutations were used to probe side-chain environment within long straight and wormlike fibrils of β_2m.** *A*, long straight fibrils (*LS*) of β_2m were formed at pH 2.5 under agitation. Wormlike fibrils (*WL*) were formed quiescently at pH 2.5 at high ionic strength. Negative stain EM images of each fibril type are shown (*scale bar*, 100 nm). *B*, sequence of β_2m showing the location of single cysteine mutations (*red*), β-strands in the native state (*black arrows*), and the disulfide bond (*heavy orange line*). *C*, location of the single cysteine mutants in the x-ray crystal structure of natively folded β_2m with strands *colored* from *blue* to *red* for strands A–G (Protein Data Bank code 1LDS (24)).

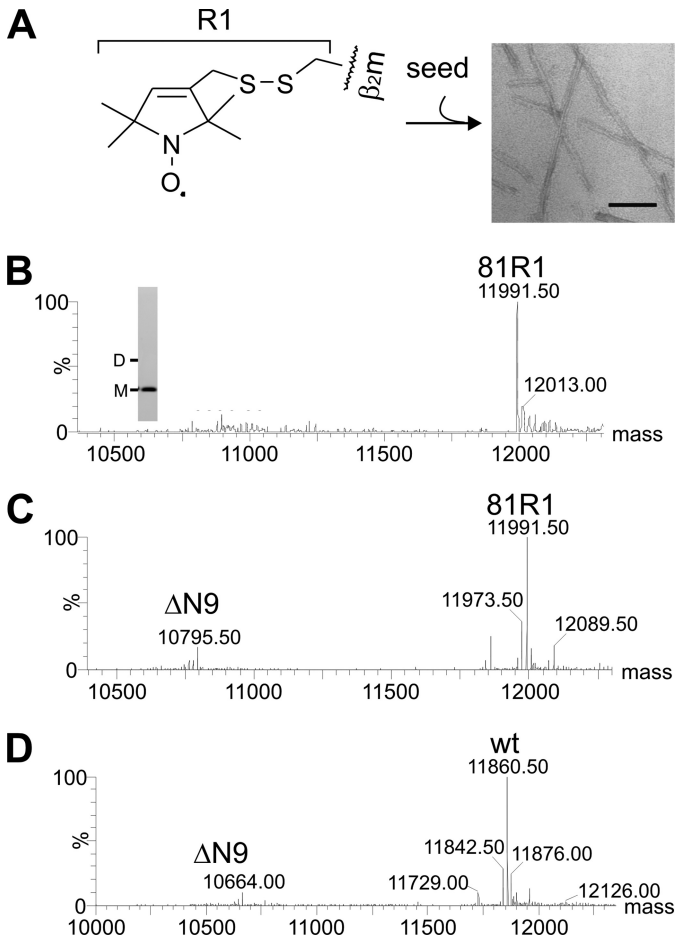

FIGURE 2. **Characterization of long straight fibrils of β_2m using limited proteolysis.** *A*, each single cysteine variant of β_2m was 100% labeled with MTSL (R1 label) and used to form long straight fibrils at pH 2.5 by seeding with fibrillar seeds created from the wild-type protein. A negative stain EM image shows fibrils formed from 81R1 (*scale bar*, 100 nm). *B*, the ESI mass spectrum of R81C 100% labeled with MTSL (81R1; expected mass, 11,991.5 Da). The *inset* shows non-reducing SDS-PAGE of 81R1 with the electrophoretic mobility of monomer (*M*) and dimer (*D*) indicated. *C*, limited proteolysis of 81R1 fibrils with pepsin for 15 min shows the main ΔN9 cleavage site. *D*, limited proteolysis of fibrils formed from wild-type β_2m (*wt*). Other cleavages found at low abundance for wild-type and 81R1 fibrils are ΔC3 (402 Da), and ΔN8 (1096 Da) (not visible at this scale).

RESULTS

Site-directed Spin Labeling and EPR of Long Straight Fibrils—In order to investigate the organization of β_2m in long straight fibrils, 19 single cysteine mutants of the protein were created, and each was quantitatively spin-labeled with MTSL (referred to as R1) (Figs. 1, *B* and *C*, and 2*A*) for analysis by EPR. The sites for mutation were selected because they are accessible according to the x-ray crystal structure of native β_2m (24) and because they provide at least one probe within each native β-strand and many of the adjoining loop regions (Fig. 1, *B* and *C*). In all cases, quantitative labeling of the newly introduced cysteine was achieved, whereas the native disulfide bond remained intact (see "Experimental Procedures"). Complete labeling was achieved as judged by ESI-MS (Fig. 2*B*). Long straight fibrils were subsequently formed from 100% labeled β_2m by seeding assembly of the labeled monomer at pH 2.5 with seeds (5% w/w) formed by assembly of the unmodified wild-type protein (see "Experimental Procedures"). Wild-type fibrils were able to seed growth of the spin-labeled variant monomer, as determined by the fibril growth kinetics monitored by thioflavin T fluorescence. Negative stain EM revealed that the spin-labeled fibrils of every variant generated in this manner have a morphology similar to that of fibrils formed from the wild-type protein (Fig. 2*A*). Limited proteolysis of the spin-labeled fibrils was also performed using the R81C and R3C variants, each 100% labeled with MTSL (named 81R1 and 3R1), and the results were compared with similar analysis of fibrils formed from the wild-type protein. Fig. 2, *C* and *D*, shows ESI mass spectra of limited proteolysis experiments on fibrils formed from 81R1 and wild-type β_2m, respectively. The results revealed a single, major cleavage site N-terminal to Tyr^{10} (releasing the product ΔN9) in both cases, with trace amounts of protein products cleaved

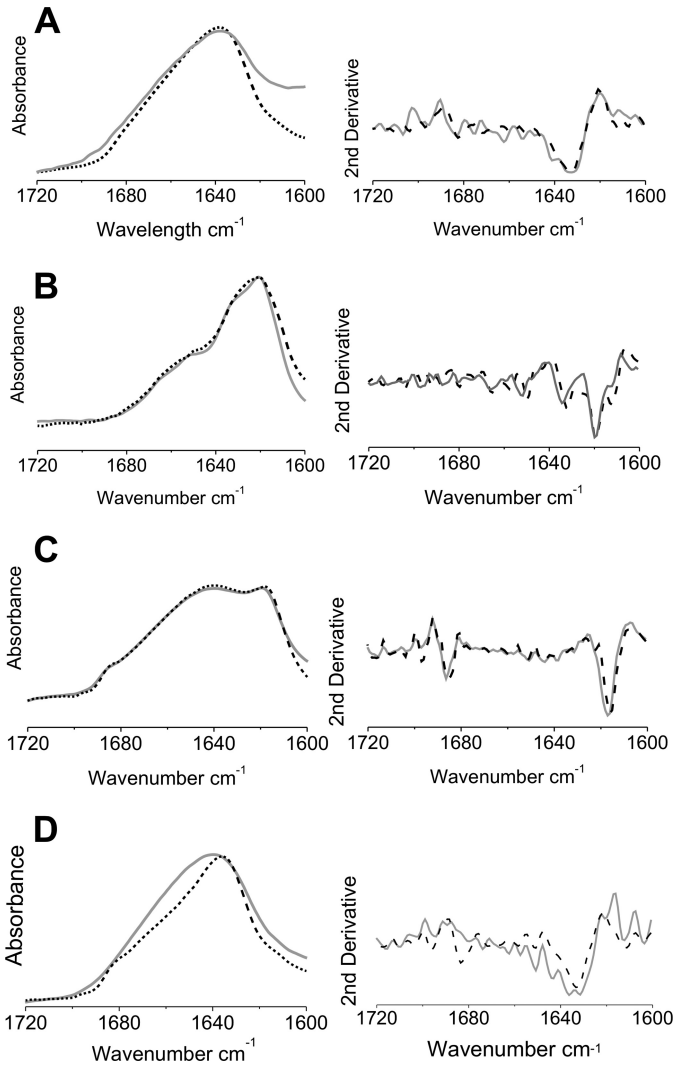

FIGURE 3. **FTIR spectra of spin labeled β_2m compared with wild-type β_2m within different assemblies.** FTIR spectra of the amide I region of wild-type β_2m (*black dashed lines*) and 61R1 β_2m (*gray lines*). *A*, the acid-unfolded monomer at pH 2.5; *B*, long straight fibrils; *C*, wormlike fibrils; *D*, ethanol precipitate at pD 2.1. *Below* each spectrum, the corresponding second derivative spectrum is shown.

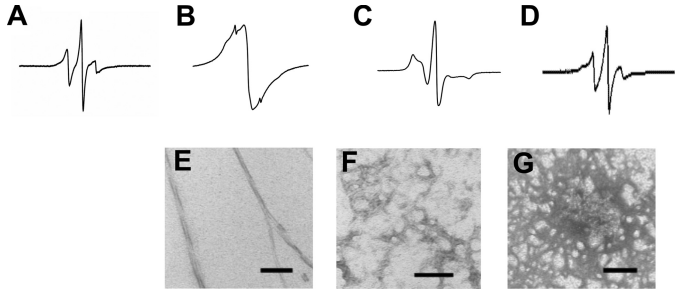

FIGURE 4. **EPR spectra and negative stain EM of different assemblies of spin-labeled β_2m.** *A–D*, EPR spectra of 73R1 within monomeric β_2m at pH 2.5 (*A*), long straight fibrils (*B*), wormlike fibrils (*C*), and ethanol precipitate at pH 2.5 (*D*). *E–G*, corresponding electron micrographs are shown for long straight fibrils (*E*), wormlike fibrils (*F*), and ethanol precipitate (*G*). *Scale bars*, 100 nm.

before Arg^{97} (ΔC3) and Val^{9} (ΔN8) (not visible in Fig. 2, *C* and *D*). The results indicate that the same core region is formed during seeded growth of fibrils from the spin-labeled variants and the wild-type protein.

As an additional control, the secondary structure content of monomers at pH 2.5, wormlike fibrils formed spontaneously by incubation at pH 2.5 with 400 mM NaCl, and long straight fibrils formed by seeded growth of spin-labeled protein at pH 2.5 were examined by FTIR, and the resulting spectra were compared with the corresponding spectra formed from wild-type β_2m (Fig. 3). The spectrum of the acid-unfolded monomer at pH 2.5 (Fig. 3*A*) has a broad amide I band centered at 1635 cm^{-1} and a broad absorbance in the region of the spectrum (1640–1650 cm^{-1}), consistent with previous results that β_2m is highly disordered at pH 2.5 (14, 25). By contrast, the FTIR spectrum of long straight fibrils is dominated by a component at 1618 cm^{-1}, characteristic of the cross-β-structure of amyloid (Fig. 3*B*) (13). Notably, the lack of a band at 1685 cm^{-1} characteristic of the anti-parallel β-sheet structure of the native protein suggests a non-native structure of β_2m in these fibrils, consistent with previous results (14, 15). The FTIR spectrum of wormlike fibrils also contains a component indicative of an intermolecular β-sheet (1616 cm^{-1}). This band is accompanied by the presence of a band at 1685 cm^{-1} and an increased contribution of disordered structure (1640–1650 cm^{-1}) compared with long straight fibrils (Fig. 3*C*). The dominance of the 1616 cm^{-1} band in the wormlike fibrils indicates that the β_2m structure within these fibrils deviates from the native structure. Finally, a control sample, formed by ethanol precipitation of acid-unfolded β_2m at pH 2.5, gives rise to a spectrum with an amide I band similar to that of acid-unfolded β_2m (Fig. 3*D*). Most importantly, these experiments indicate that the presence of the spin label does not affect the fibril architecture for any of the assemblies studied, at least within the resolution of FTIR.

To gain information about the environment and mobility of the side chains in different β_2m conformations, EPR spectra of the spin-labeled β_2m samples in solution in the monomeric state as well as when assembled into different fibrillar structures were obtained. As illustrated for the 73R1 derivative (Fig. 4*A*), the EPR spectrum of monomer at pH 2.5 (in 30% sucrose) results in sharp and narrowly spaced spectral lines indicating high mobility. Similar results were obtained for all other sites (not shown), consistent with the disordered structure that is generated under these conditions (25). Upon formation of long straight fibrils (Fig. 4, *B* and *E*), a very different EPR spectrum is obtained. This spectrum is dominated by a single spectral line that is indicative of spin exchange narrowing. Such spin exchange is caused by the close proximity of multiple spin labels, previously estimated to be within 7 Å of each other, and causes the loss of well defined three-line hyperfine structure (26). The EPR spectrum of 73R1 in long straight fibrils is highly reminiscent of the spectra obtained for residues in a parallel, in-register structure of fibrils formed from α-synuclein (27), human recombinant prion protein (28), Tau (29), and islet amyloid polypeptide (30). In contrast, wormlike fibrils assembled from 73R1 give rise to an EPR spectrum that can be characterized as moderately immobilized with relatively little spin-spin interaction (Fig. 4, *C* and *F*). Thus, at least in this region of the sequence, wormlike fibrils have a structural organization that is distinct from that within long straight fibrils of β_2m. As a control, we also generated an ethanol-precipitated 73R1 variant at

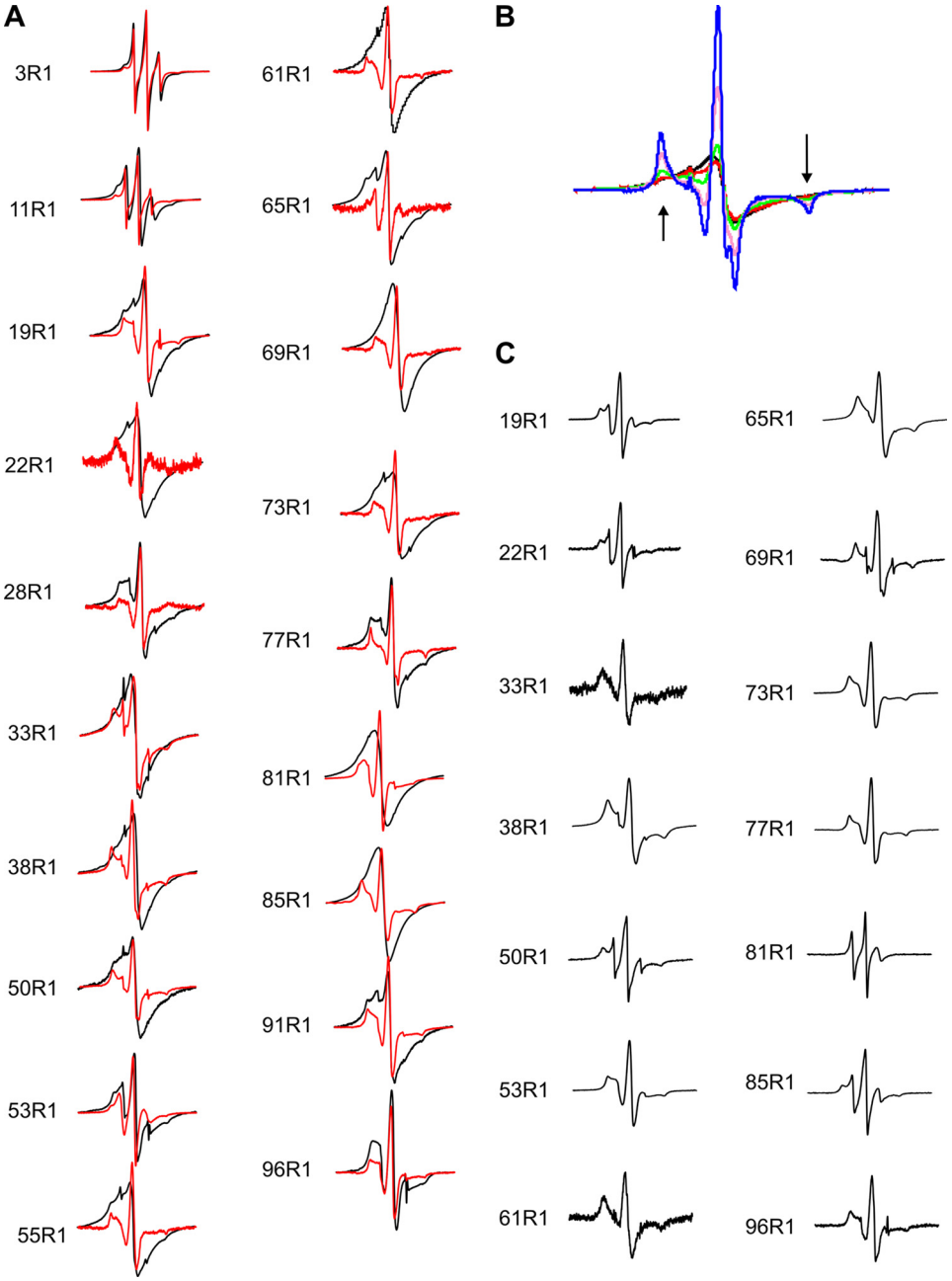

FIGURE 5. **EPR spectra of spin-labeled β_2m within long straight and wormlike fibrils.** *A*, EPR spectra of fibrils formed from 100% R1-labeled β_2m (*black*) or 25% R1-labeled β_2m and 75% wild-type β_2m (*red*), with spectra normalized to amplitude. *B*, overlay of EPR spectra of fibrils formed from different quantities of 61R1 and wild-type β_2m monomers with 100% R1 (*black line*), 75% R1 (*red line*), 50% R1 (*green line*), 25% R1 (*pink line*), and 10% R1 (*blue line*) normalized to the same number of spins. The *arrows* point to the emerging hyperfine peaks that increase in intensity as the dilution of the spin label is increased in the different samples. *C*, wormlike fibrils of β_2m formed at pH 2.5 in 0.4 M NaCl with 100% R1. All EPR spectra were obtained at room temperature using a 150 gauss scan width.

pH 2.5 and found that the EPR spectrum is distinctively different from that of both fibril types (Fig. 4, *D* and *G*).

Exchange Narrowing Indicates a Parallel, In-register Organization of the Polypeptide Chain in Long Straight Fibrils of β_2m—To investigate the extent to which the long straight fibrils of β_2m have a parallel, in-register organization, EPR spectra of fibrils formed from 19 different single cysteine variants, each 100% labeled with MTSL, were acquired (Fig. 5*A*). Exchange-narrowed EPR spectra were observed for most sites in the core region, which was previously defined by limited proteolysis and hydrogen/deuterium exchange as involving approximately residues 20–87 (8, 11). The most pronounced single line EPR spectra were obtained for labels introduced at positions 61, 81, and 85. To illustrate the exchange narrowing, a series of samples were created in which the spin label was diluted by forming fibrils from varying amounts of spin-labeled and wild-type protein. Spin dilution suppresses the exchange narrowing and restores hyperfine structure (note the emerging outer peaks for 10 and 25% labeling for the 61R1 variant, denoted by *arrows* in Fig. 5*B*). Analogous spectral changes were reported previously for spin dilution of α-synuclein and Tau fibrils and are clear indications of spin exchange narrowing (26, 29). With the exception of positions 28, 53, and 77, the spectra of all other sites labeled to 100% with MTSL in the core region of the β_2m fibrils are dominated by single line, exchange-narrowed EPR spectra. Thus, the core region has extensive segments in which the same residues come into close contact with each other, indicative of a parallel, in-register structure.

In contrast with the strong spin exchange observed at 16 sites within the core region, little or no detectable spin exchange is apparent in the EPR spectra for spin labels introduced in the N-terminal or C-terminal regions of the polypeptide chain (3R1, 11R1, and 96R1), indicating the absence of a parallel, in-register stacking at these residues. The EPR spectra for 19R1 and 91R1, two sites in regions flanking the core region, retain detectable exchange narrowing, suggesting that at least some parallel, in-register structure extends beyond the core region mapped by hydrogen/deuterium exchange.

In order to compare the structural architecture of the long straight fibrils of β_2m with that of wormlike fibrils, spin-labeled derivatives were also assembled into wormlike fibrils at pH 2.5 by the addition of 0.4 M NaCl (3) and verified by EM (Figs. 1*A* and 4*F*). The EPR line shapes of all sites investigated in wormlike fibrils are dominated by spectral broadening that occurs as a consequence of immobilization rather than from the pro-

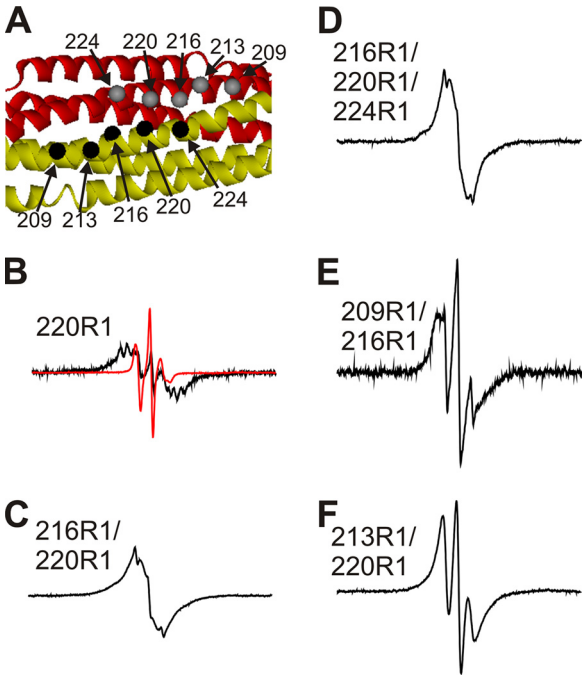

FIGURE 6. **Spin-spin interactions in R1-labeled amphiphysin dimers.** *A*, the crystal structure of the amphiphysin dimer indicates the positions at which spin labels were introduced (Protein Data Bank code 1URU (31)). The different subunits are shown as *red* and *gold ribbons*, and the α-carbon positions of the spin-labeled sites are given as *gray* and *black spheres*. *B–F*, EPR spectra of indicated derivatives obtained at room temperature. The *black spectra* are from 100% R1-labeled proteins. The *red spectrum* for the 220R1 derivative was obtained at 15% R1 labeling and is shown for comparison at 10-fold reduced amplitude (*B*). The scan width for all spectra is 300 gauss. These spectra are normalized to the same number of spins.

nounced spin-spin interactions that are observed when spin labels are aligned in close proximity (Fig. 5*C*). Although some minor components of spin-spin interaction may be present for 38R1 and 65R1, none of the spectra exhibit strong spin-spin interaction or any detectable exchange narrowing. The data thus indicate that the wormlike fibrils of β_2m do not adopt a tightly packed parallel, in-register structure, as observed for the long straight fibrils, consistent with the very different tinctorial, FTIR, and antibody binding properties of these fibril types (5–7).

Four Stacked Spin Labels Are Sufficient to Generate Exchange-narrowed Single Line Spectra—Although models based on an indefinite number of β-strands in a parallel, in-register arrangement are consistent with the present data, the discontinuous nature of the electron density observed in cryo-EM three-dimensional maps of long straight fibrils of β_2m (16) are inconsistent with such a model; *i.e.* the cryo-EM structure indicates that the number of stacked strands must be limited in fibrils of β_2m so as to explain the subunit repeat of ~6 nm clearly revealed as a distinctive feature of the β_2m fibril structure. To determine the number of β-strands in a parallel, in-register array required to produce single line EPR spectra, amphiphysin (a stable dimeric α-helical protein) was used as a model system (Fig. 6*A*). In an α-helical protein, the spacing per turn is 5.4 Å, a distance that is slightly longer than, but still comparable with, that expected from a parallel, in-register structure in an amyloid fibril (4.7 Å). Two, four, or six spin labels were therefore placed at different distances within the well known amphiphysin structure to investigate the distances between and the number of spin labels required to generate exchange narrowing.

An example of the spin-spin interaction obtained for the 220R1 derivative of amphiphysin is shown in Fig. 6*B*. This residue is near a 2-fold symmetry axis (Fig. 6*A*) in the dimer and within 5.6 Å of the neighboring residue (α-carbon distance) in the adjacent subunit (31). Unlike the control spectrum of spin-diluted 220R1 (*red trace* shown at 10-fold reduced amplitude in Fig. 6*B*), the spectrum of fully labeled amphiphysin (*black trace*) is strongly broadened and low in spectral amplitude. The most significant spectral components are shifted to the high field and low field regions, and the spectral intensity near the central line is substantially reduced. These spectral effects are consistent with strong dipolar broadening and confirm the notion that exchange narrowing is not observed for two spin labels in close contact (26).

In contrast, the 216R1/220R1 derivative gives rise to a spectrum that is less broadened and exhibits significant intensity in the central region of the spectrum (Fig. 6*C*). In fact, aside from a relatively minor spectral component with sharp lines, the overall shape of this spectrum can be described as exchange-narrowed. According to the crystal structure of amphiphysin, the α-carbon distances between those residues are between 5 and 6 Å, and, considering that these side chains (as well as the others chosen here) are projecting in the same direction, a similar average distance can be expected for the internitroxide distances (32). Thus, four spin labels in close proximity can give rise to spectral line shapes indicative of spin exchange narrowing. In the 216R1/220R1/224R1 derivative, six spin labels are expected to come into close proximity, and this derivative also results in a spectrum with an overall line shape similar to that of the 216R1/220R1 derivative (Fig. 6*D*).

Having shown that close contact ($\leq$7 Å) of four or more spin labels can give rise to EPR spectra with characteristic exchange-narrowed features, two additional variants of amphiphysin were generated to determine whether four spin labels can give rise to exchange narrowing when spaced further apart. In the 209R1/216R1 variant, the α-carbon distances for residues 209 and 216 are 10 Å, whereas the cross-dimer distance for 216 is 14 Å. The resulting spectrum exhibits dipolar broadening rather than spin exchange interaction (Fig. 6*E*). Next we asked whether exchange narrowing can occur when two labels are in close contact while the other two labels are about 10 Å apart. This notion was tested using the 213R1/220R1 double-labeled variant. This derivative also showed no detectable signs of spin exchange narrowing (Fig. 6*F*). Taken together, the data indicate that a series of four spin labels in close contact ($\leq$7 Å) is sufficient for spin exchange to occur. This serves as a useful restraint for building models of the cross-β structure of amyloid as well as other macromolecular assemblies that give rise to single line EPR spectra.

Mobility of Spin-labeled Side Chains—To obtain additional information about the mobility of the side chains in the spin-labeled derivatives of long straight fibrils of β_2m, additional dilution experiments were performed in which 25% of spin-labeled β_2m variants were each mixed with 75% wild-type monomer prior to seeded fibril elongation. Under these conditions,

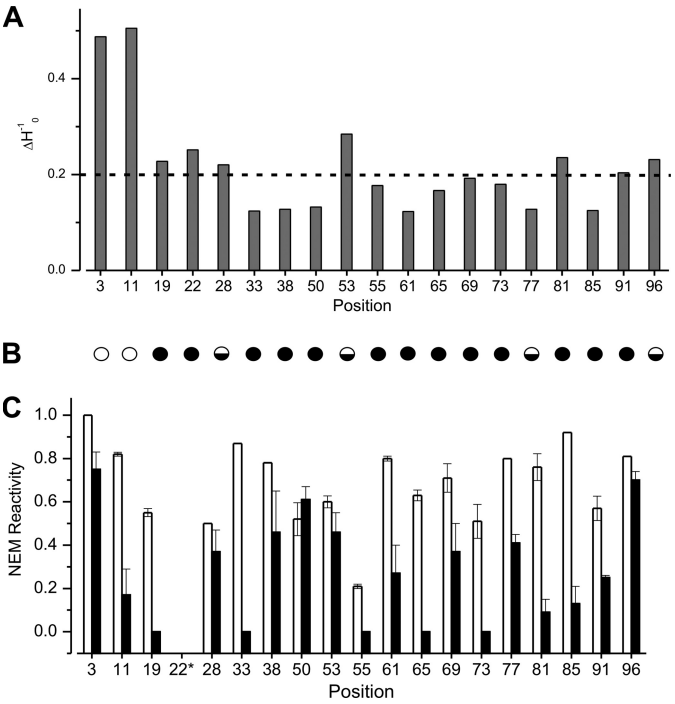

FIGURE 7. **Mobility and NEM reactivity of different residues in long straight fibrils of β_2m.** *A*, mobility measured from inverse central line width (ΔH_0^{-1}). The *dashed line* at 0.2 gauss^{-1} represents the value expected for buried side chains. *B*, representation of the absence (*empty circle*), presence (*filled circle*), or partial (*half-filled circle*) exchange narrowing in EPR spectra of 100% R1-labeled samples. *C*, NEM reactivity of cysteine residues in the native monomer (*white*) and long straight fibrils (*black*) determined using ESI-MS. *Error bars* are from two or three replicates of the NEM labeling procedure conducted with separate fibril samples. *, although 22R1 formed fibrils with high yield, the unlabeled counterpart (F22C) did not form fibrils under the conditions used.

the line shape of the resulting fibrils should be dominated by mobility rather than spin-spin interaction as long as the spin-labeled variant and wild-type monomer co-assemble (29). Examination of EPR spectra of 25% spin-labeled fibrils indicated that most sites (with the exception of 53R1 and 81R1) reveal significant immobilization for the spin-labeled side chains within the core of the long straight fibrils (Fig. 5*A*). Among the residues N-terminal and C-terminal to this region, immobilization that is consistent with β-sheet structure is observed for 19R1 and 91R1, which immediately flank the core. The only positions with EPR spectra that display very sharp lines among all of the sites tested are residues 3 and 11. These lines indicate high mobility that is typically observed for side chains in loop regions of the polypeptide chain (33).

The mobility information contained within the EPR spectra of the long straight fibrils of β_2m is summarized using the inverse of the central line width in Fig. 7*A*. The mobility of most sites in the core region have ΔH_0^{-1} values below 0.2 gauss^{-1} (indicated by a *dashed line*), consistent with buried side chains in model β-sheet (34, 35) and α-helical proteins (33, 36, 37). Strong immobilization and low ΔH_0^{-1} values were also obtained in spin labeling experiments of fibrils formed from Aβ 1–40, α-synuclein, and Tau (27, 29, 38). Position 53 in fibrils of β_2m has the highest mobility of all residues measured within the fibril core region, with a ΔH_0^{-1} value that is even higher than that found for resides in the turn region of Aβ 1–40 fibrils (38, 39). Combined with the strongly reduced presence of spin exchange at this position (Figs. 5*A* and 7*B*), the data suggest that position 53 is in an exposed turn position in β_2m amyloid fibrils. Positions 3 and 11 have the highest mobility in the fibril structure, with ΔH_0^{-1} values near 0.5, which is consistent with more dynamic structural components in this region.

NEM Labeling of Long Straight β_2m Fibrils—More information about the environment and accessibility of side chains within the long straight fibrils of β_2m was obtained by determining the ability of each newly introduced cysteine residue to react with NEM. The fibrils formed from each unmodified cysteine variant were confirmed to have the same morphology as fibrils formed from the wild-type protein by negative stain EM and to have similar β-sheet organization, as measured using FTIR (data not shown). Fibrils from single cysteine variants formed at pH 2.5 were then labeled with a 100-fold molar excess of NEM for 10 min at pH 7 and then immediately returned to pH 2.5 and prepared for analysis by ESI-MS. Control experiments demonstrated that most of the fibrils remain intact after labeling for 10 min at pH 7 and that labeling occurs specifically at the newly introduced cysteine residue in protein chains distributed throughout the fibril structure and not just at the more dynamic fibril ends (see "Experimental Procedures").

The percentages of labeling with NEM for the native monomer and fibrils formed from 18 of the cysteine variants generated are shown in Fig. 7*C*. The results show that high NEM reactivity is observed for cysteine residues in the N-terminal and C-terminal regions of the polypeptide chains (residues 3 and 96) in the fibril sample, whereas the reactivity of residues located within the amyloid core varies from zero (residues 19, 33, 55, 65, and 73), suggestive of completely inaccessible sites, to values similar to that obtained for the monomer (residues 28, 50, and 53). Notably, position 11 has low reactivity to NEM compared with monomeric β_2m (Fig. 7*C*), despite its high spin label mobility, nearness to the pepsin cleavage site after residue 9, and weak protection from hydrogen/deuterium exchange behavior (9, 11). The reactivity to NEM labeling of the region 20–87 shows that side chains in the core are not packed tightly enough to exclude penetration of NEM, although the backbone amides are protected from proteolysis and have hydrogen/deuterium exchange protection factors of $\sim 10^3$ to 10^4 and spin-labeled side chains stacked closely enough to be in spin exchange. Positions 50 and 53 have NEM reactivity that is among the highest of all sites tested in the fibril core region. These residues display the same extent of labeling with NEM as the native monomer, supporting the view that side chains at these positions are dynamic and in a solvent-exposed region. The different NEM reactivity of residues within the amyloid core is consistent with the view that the cross-β-structure of β_2m fibrils contains regions that have tightly packed dry interfaces interspersed with regions where side chains are ordered but remain solvent-accessible.

DISCUSSION

Stacked Sets of Parallel, In-register Arrays Dominate the Structural Organization of Long Straight β_2m Fibrils—Recent cryo-EM three-dimensional maps suggest that β_2m fibrils contain a complex structure involving multiple interfaces and pro-

tofibrils composed of stacked dimer-of-dimer repeats (16). Here we have used EPR and NEM reactivity of individual cysteine variants to provide residue-specific information about the structural organization of the polypeptide chains of β_2m within these amyloid fibrils. Based on the presence of exchange narrowing in EPR spectra of spin-labeled variants that starts at residue 19 and continues to position 91, the structural organization of β_2m in long straight fibrils is revealed as a parallel, in-register arrangement involving much of the polypeptide chain and indicates that β_2m must adopt a highly non-native structure in these fibril types. The pattern of exchange narrowing in the EPR spectra of β_2m fibrils shown here is only broken at positions 28R1, 53R1, and 77R1, for which hyperfine peaks are seen with a lesser component of spin exchange than other positions in the core, providing a limit to the strand lengths within the fibril structure (Fig. 7*A*). Given the number of sites studied here, however, a detailed map of β-strand boundaries is not possible. Other amyloid fibrils characterized by site-directed spin labeling EPR, including Aβ 1–40, Aβ 1–42, Tau, α-synuclein, human recombinant prion protein, and islet amyloid polypeptide (27, 28, 30, 38, 40) have also been shown to contain a parallel, in-register structure. In addition, solid state NMR has demonstrated a parallel in-register arrangement for amyloid fibrils, including Aβ 1–40, islet amyloid polypeptide, prion protein residues 106–126, and the K3 fragment of β_2m (residues 20–41) (41–44).

The arrangement of β_2m in long straight fibrils differs from the organization within wormlike fibrils, which were shown here to have no evidence for spin exchange in any of the sites tested. The lack of single line exchange-narrowed spectra in wormlike fibrils, together with the presence of a 1685 cm^{-1} band in the FTIR spectra, is consistent with a structure for these fibrils based on stacking of native-like subunits of β_2m, although models based on anti-parallel structures that deviate from the native structure are also consistent with the data presented.

It is well established that exchange narrowing requires multiple spin labels that are within orbital overlap of each other (26). Because orbital overlap decays exponentially, such spin labels must be in close proximity for such a spectrum to occur. Analysis of the literature of spin exchange in various systems has shown that spin labels must be within 7 Å to obtain exchange-narrowed spectra (26). In human recombinant PrP fibrils, it was demonstrated that if spin labels are out of register by only a single position, then single line exchange-narrowed spectra are not obtained (28). The precise number of spin labels required to give exchange narrowing, however, remained unknown. Here we show, using amphiphysin as a model, that two closely contacting spin labels give rise to spectral lines with strong dipolar broadening but no spin exchange narrowing. By contrast, four or more spin labels spaced ~5 to 6 Å apart give rise to significant exchange narrowing. The exchange-narrowed lines observed here for amphiphysin are qualitatively similar to those found in long straight fibrils formed from β_2m, showing that four or more spin labels stacked within <7 Å of each other are sufficient to generate exchange narrowing. Importantly, in the derivatives of amphiphysin in which the distances between spin labels are ≥10 Å, no exchange narrowing was detected. This reiterates the steep distance dependence of spin exchange and further illustrates that spin exchange at multiple sites could not be caused by an anti-parallel structure. These data support the conclusion that β_2m adopts a highly non-native conformation within the long straight fibrils that is arranged in stacked sets of parallel, in-register chains.

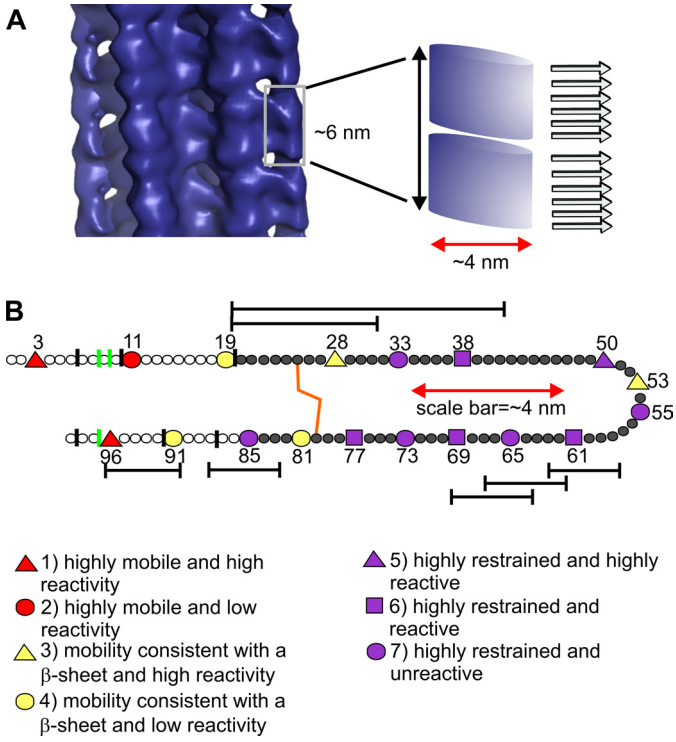

FIGURE 8. **Long straight fibrils of β_2m are arranged as sets of β-strands stacked in parallel, in-register repeats.** *A*, the subunit repeat shown by cryo-EM of β_2m fibrils (16) indicates that there must be a break in the parallel in-register arrangement of the constituent β-strands within the cross-β-array. Here two sets of six β-strands are proposed to fit into the ~6-nm repeat. Such an arrangement is fully consistent with residues in these strands giving rise to single line EPR spectra. *B*, side-chain environment, based on spin label mobility and NEM reactivity, classified as indicated in the figure and as described under "Discussion." The *red scale bars* in *A* and *B* depict the diameter of the subunit as observed in the cryo-EM structure. This highlights that each subunit cannot accommodate an entire β_2m monomer in a cross-β-orientation with a fully extended conformation as shown schematically in *B*. The *vertical green lines* indicate pepsin cut sites (this work and Ref. 9), and *vertical black lines* indicate cleavage sites observed using different proteases (8). Hydrogen/deuterium exchange protection of the fibril core is shown as *dark gray filled circles*, and reduced protection in N-terminal and C-terminal region is shown as *white circles* (11). The disulfide bond is shown in *orange*. Hexameric peptide fragments, in addition to the K3 peptide and a peptide containing residues 20–31 that form amyloid-like fibrils in isolation are indicated as *bars* spanning the residues involved (51–53). Other larger peptides covering these same regions form amyloid (54) but are not shown here for clarity. Note that most of the peptide sequences with an intrinsic amyloid potential, except for one peptide at the C-terminal, are found within structured regions in the amyloid fibril formed from the intact protein (*B*).

The minimal number of spin labels capable of yielding exchange-narrowed EPR spectra has important implications for understanding the arrangement of β_2m in the cryo-EM structure of long straight β_2m fibrils (16). Based on the data presented here, we propose that the subunit repeat observed in the cryo-EM structure of β_2m fibrils, which varies from 5.2 to 6.5 nm in height in different fibrils, is composed of two stacks of about six β-strands organized in a parallel and in-register array along the fibril axis (Fig. 8*A*). A break in the parallel in-register arrangement is required to be consistent with the subunit

repeat structure observed by cryo-EM. Importantly, as shown using amphiphysin as a model, an organization with six spin labels in close proximity would give rise to a single line EPR spectrum. These data thus provide new insights into the architecture of amyloid fibrils as containing both a subunit repeat and a parallel, in-register stacking of β-strands. How the protein chains fit into the globular-like domains of the cryo-EM structure remains unknown and, given the complexity of the structure and the limited number of restraints available, cannot yet be deduced. However, the combination of EPR and NEM reactivity shown here reveals a fibril structure in which a large proportion of the polypeptide chain is organized in a stacked parallel, in-register array that is highly non-native.

Side Chain Dynamics and Solvent Exposure in Long Straight Fibrils of β_2m—In addition to the parallel, in-register arrangement of β_2m in long straight fibrils, side chain mobility and accessibility data presented here show that many side chains in the fibrils are solvent-accessible and dynamic, including several within the amyloid core. The combination of the spin-label mobility and NEM reactivity were used to classify the side-chain positions into different classes (Fig. 8*B*). Based on their inverse central line widths being above 0.4 gauss^{-1}, above 0.2 gauss^{-1}, or below 0.2 gauss^{-1}, sites were considered highly dynamic, intermediate, or strongly immobilized, respectively. Similarly, NEM reactivity above 75%, above 30%, or below 30% (compared with monomer reactivity) was used to classify sites as highly reactive, reactive, or minimally reactive. Guided by these criteria, the side-chain classes are defined as: 1) highly dynamic and highly reactive to NEM (positions 3 and 96); 2) highly dynamic but minimally reactive (position 11); 3) having dynamics consistent with a solvent-exposed side chain in a location on a β-sheet and high reactivity (position 28 and 53); 4) having β-sheet-like dynamics and minimal reactivity (position 19, 81 and 91); 5) highly restrained but highly reactive (position 50); 6) highly restrained but reactive (positions 38, 61, 69, and 77); and 7) highly restrained and having low NEM reactivity (position 33, 55, 65, 73, and 85). Fig. 8*B* highlights that the side chains of residues in the N-terminal and C-terminal regions of the protein chain (class 1) are solvent-exposed and unrestrained in the amyloid fold, despite the main-chain retaining order, as revealed by protection factors of 10^2–10^3, scarcity of protease digestion sites, and lack of peaks in solution NMR (8, 10, 12). Position 53 has the highest mobility of all residues analyzed in the amyloid core, suggesting that this residue is in a solvent-exposed loop structure. No information is available for the hydrogen exchange protection for this residue (10), so whether the main-chain is also dynamic remains unknown. In contrast, residues 38, 50, 61, 69, and 77 lie in classes 5 and 6, which suggest that these residues participate in a restrained β-sheet structure, which, however, does not prevent access to NEM. Such NEM reactivity, combined with low side chain mobility in the core, suggests that these residues are in wet interfaces in the fibril. Finally, positions 33, 55, 65, 73, and 85 (class 7) are consistent with these residues forming the most tightly packed region with a dry interface. Although this information gives insight into the dynamics and accessibility of the side chains, we are not able to model how the polypeptide folds within the stacked sets of parallel, in-register structure from the limited number of restraints available.

The view of amyloid-like fibrils of β_2m that emerges from these studies is a complex structure involving a highly organized backbone in which much of the polypeptide chain forms a parallel, in-register structure. This structure contains regions with well packed side chains interspersed with dynamic side chains. Such a model is consistent with previous studies using pressure-induced unfolding and density measurements, which indicate that long straight fibrils are less tightly packed than natively folded β_2m (45, 46), and information from cryo-EM, which shows large, open cavities between protofilaments (Fig. 8*A*). Complexity in the fibril structure is also seen by biphasic hydrogen/deuterium exchange kinetics of the N-terminal and C-terminal regions (11). This heterogeneity is reinforced by the presence of two components in the 25% spin-labeled EPR spectra of residues 3R1 and 11R1. The immobilized components for both positions are seen as a small broadened outer peak, nearly overwhelmed by the mobile component. This immobile component may reflect close range interactions with adjacent side chains or a more substantial conformational change in the backbone that alters the side chain packing of N-terminal region. Cryo-EM of β_2m long straight fibrils also shows heterogeneity both in the arrangement of the protofilaments and in the crossover repeat length in fibrils formed within a single sample under defined growth conditions (16). These results contribute to the view that the structure of β_2m long straight fibrils is complex and heterogeneous. Taken together with the data presented here, we propose that each protofilament contains stacks of about six β-strands organized in a parallel in-register arrangement consistent with a subunit repeat of ~6 nm revealed by cryo-EM (Fig. 8*A*) (16). This complex structure for an amyloid fibril is in marked contrast with the dense, ordered cross-β-array proposed for other amyloid fibrils (39, 44, 47–50). Whether such a structure is unique to β_2m fibrils or is more widespread awaits further detailed studies of other fibril types.

Acknowledgments—We thank Prof. Alison Ashcroft and Dr. James Ault for guidance in mass spectrometry, Dr. Harvey McMahon for providing the amphiphysin expression construct, Prof. Alan Berry for FTIR, Timo Eichner for ^{15}N-labeled β_2m, and Dr. Wei-Feng Xue for advice on reactivity data analysis. We thank Prof. Helen Saibil for many helpful discussions that shaped the study and for providing the coordinates of the cryo-EM structure.

REFERENCES

1. Gejyo, F., Yamada, T., Odani, S., Nakagawa, Y., Arakawa, M., Kunitomo, T., Kataoka, H., Suzuki, M., Hirasawa, Y., Shirahama, T., Cohen, A. S., and Schmid, K. (1985) *Biochem. Biophys. Res. Commun.* **129,** 701–706
2. Platt, G. W., and Radford, S. E. (2009) *FEBS Lett.* **583,** 2623–2629
3. Gosal, W. S., Morten, I. J., Hewitt, E. W., Smith, D. A., Thomson, N. H., and Radford, S. E. (2005) *J. Mol. Biol.* **351,** 850–864
4. Xue, W. F., Homans, S. W., and Radford, S. E. (2008) *Proc. Natl. Acad. Sci. U.S.A.* **105,** 8926–8931
5. Smith, D. P., Jones, S., Serpell, L. C., Sunde, M., and Radford, S. E. (2003) *J. Mol. Biol.* **330,** 943–954
6. McParland, V. J., Kad, N. M., Kalverda, A. P., Brown, A., Kirwin-Jones, P., Hunter, M. G., Sunde, M., and Radford, S. E. (2000) *Biochemistry* **39,**

8735–8746
7. Xue, W. F., Hellewell, A. L., Gosal, W. S., Homans, S. W., Hewitt, E. W., and Radford, S. E. (2009) *J. Biol. Chem.* **284,** 34272–34282
8. Monti, M., Amoresano, A., Giorgetti, S., Bellotti, V., and Pucci, P. (2005) *Biochim. Biophys. Acta.* **1753,** 44–50
9. Myers, S. L., Thomson, N. H., Radford, S. E., and Ashcroft, A. E. (2006) *Rapid Commun. Mass Spectrom.* **20,** 1628–1636
10. Hoshino, M., Katou, H., Hagihara, Y., Hasegawa, K., Naiki, H., and Goto, Y. (2002) *Nat. Struct. Biol.* **9,** 332–336
11. Yamaguchi, K., Katou, H., Hoshino, M., Hasegawa, K., Naiki, H., and Goto, Y. (2004) *J. Mol. Biol.* **338,** 559–571
12. Platt, G. W., Xue, W. F., Homans, S. W., and Radford, S. E. (2009) *Angew. Chem. Int. Ed. Engl.* **48,** 5705–5707
13. Fändrich, M., and Dobson, C. M. (2002) *EMBO J.* **21,** 5682–5690
14. Fabian, H., Gast, K., Laue, M., Misselwitz, R., Uchanska-Ziegler, B., Ziegler, A., and Naumann, D. (2008) *Biochemistry* **47,** 6895–6906
15. Kardos, J., Okuno, D., Kawai, T., Hagihara, Y., Yumoto, N., Kitagawa, T., Závodszky, P., Naiki, H., and Goto, Y. (2005) *Biochim. Biophys. Acta* **1753,** 108–120
16. White, H. E., Hodgkinson, J. L., Jahn, T. R., Cohen-Krausz, S., Gosal, W. S., Müller, S., Orlova, E. V., Radford, S. E., and Saibil, H. R. (2009) *J. Mol. Biol.* **389,** 48–57
17. Chiba, T., Hagihara, Y., Higurashi, T., Hasegawa, K., Naiki, H., and Goto, Y. (2003) *J. Biol. Chem.* **278,** 47016–47024
18. Kihara, M., Chatani, E., Iwata, K., Yamamoto, K., Matsuura, T., Nakagawa, A., Naiki, H., and Goto, Y. (2006) *J. Biol. Chem.* **281,** 31061–31069
19. Hong, D. P., Gozu, M., Hasegawa, K., Naiki, H., and Goto, Y. (2002) *J. Biol. Chem.* **277,** 21554–21560
20. Kad, N. M., Thomson, N. H., Smith, D. P., Smith, D. A., and Radford, S. E. (2001) *J. Mol. Biol.* **313,** 559–571
21. Qoronfleh, M. W., Hesterberg, L. K., and Seefeldt, M. B. (2007) *Protein Expr. Purif.* **55,** 209–224
22. Margittai, M., and Langen, R. (2006) *Methods Enzymol.* **413,** 122–139
23. Smith, D. P., and Radford, S. E. (2001) *Protein Sci.* **10,** 1775–1784
24. Trinh, C. H., Smith, D. P., Kalverda, A. P., Phillips, S. E., and Radford, S. E. (2002) *Proc. Natl. Acad. Sci. U.S.A.* **99,** 9771–9776
25. Platt, G. W., McParland, V. J., Kalverda, A. P., Homans, S. W., and Radford, S. E. (2005) *J. Mol. Biol.* **346,** 279–294
26. Margittai, M., and Langen, R. (2008) *Q. Rev. Biophys.* **41,** 265–297
27. Chen, M., Margittai, M., Chen, J., and Langen, R. (2007) *J. Biol. Chem.* **282,** 24970–24979
28. Cobb, N. J., Sönnichsen, F. D., McHaourab, H., and Surewicz, W. K. (2007) *Proc. Natl. Acad. Sci. U.S.A.* **104,** 18946–18951
29. Margittai, M., and Langen, R. (2004) *Proc. Natl. Acad. Sci. U.S.A.* **101,** 10278–10283
30. Jayasinghe, S. A., and Langen, R. (2004) *J. Biol. Chem.* **279,** 48420–48425
31. Peter, B. J., Kent, H. M., Mills, I. G., Vallis, Y., Butler, P. J., Evans, P. R., and McMahon, H. T. (2004) *Science* **303,** 495–499
32. Jao, C. C., Hegde, B. G., Chen, J., Haworth, I. S., and Langen, R. (2008) *Proc. Natl. Acad. Sci. U.S.A.* **105,** 19666–19671
33. Mchaourab, H. S., Lietzow, M. A., Hideg, K., and Hubbell, W. L. (1996) *Biochemistry* **35,** 7692–7704
34. Lietzow, M. A., and Hubbell, W. L. (2004) *Biochemistry* **43,** 3137–3151
35. Koteiche, H. A., Berengian, A. R., and Mchaourab, H. S. (1998) *Biochemistry* **37,** 12681–12688
36. Isas, J. M., Langen, R., Haigler, H. T., and Hubbell, W. L. (2002) *Biochemistry* **41,** 1464–1473
37. Margittai, M., Fasshauer, D., Pabst, S., Jahn, R., and Langen, R. (2001) *J. Biol. Chem.* **276,** 13169–13177
38. Török, M., Milton, S., Kayed, R., Wu, P., McIntire, T., Glabe, C. G., and Langen, R. (2002) *J. Biol. Chem.* **277,** 40810–40815
39. Petkova, A. T., Ishii, Y., Balbach, J. J., Antzutkin, O. N., Leapman, R. D., Delaglio, F., and Tycko, R. (2002) *Proc. Natl. Acad. Sci. U.S.A.* **99,** 16742–16747
40. Margittai, M., and Langen, R. (2006) *J. Biol. Chem.* **281,** 37820–37827
41. Balbach, J. J., Petkova, A. T., Oyler, N. A., Antzutkin, O. N., Gordon, D. J., Meredith, S. C., and Tycko, R. (2002) *Biophys. J.* **83,** 1205–1216
42. Luca, S., Yau, W. M., Leapman, R., and Tycko, R. (2007) *Biochemistry* **46,** 13505–13522
43. Walsh, P., Simonetti, K., and Sharpe, S. (2009) *Structure* **17,** 417–426
44. Iwata, K., Fujiwara, T., Matsuki, Y., Akutsu, H., Takahashi, S., Naiki, H., and Goto, Y. (2006) *Proc. Natl. Acad. Sci. U.S.A.* **103,** 18119–18124
45. Chatani, E., Kato, M., Kawai, T., Naiki, H., and Goto, Y. (2005) *J. Mol. Biol.* **352,** 941–951
46. Lee, Y. H., Chatani, E., Sasahara, K., Naiki, H., and Goto, Y. (2009) *J. Biol. Chem.* **284,** 2169–2175
47. Sawaya, M. R., Sambashivan, S., Nelson, R., Ivanova, M. I., Sievers, S. A., Apostol, M. I., Thompson, M. J., Balbirnie, M., Wiltzius, J. J., McFarlane, H. T., Madsen, A. Ø., Riekel, C., and Eisenberg, D. (2007) *Nature* **447,** 453–457
48. Wasmer, C., Lange, A., Van Melckebeke, H., Siemer, A. B., Riek, R., and Meier, B. H. (2008) *Science* **319,** 1523–1526
49. van der Wel, P. C., Lewandowski, J. R., and Griffin, R. G. (2007) *J. Am. Chem. Soc.* **129,** 5117–5130
50. Nelson, R., Sawaya, M. R., Balbirnie, M., Madsen, A. Ø., Riekel, C., Grothe, R., and Eisenberg, D. (2005) *Nature* **435,** 773–778
51. Ivanova, M. I., Thompson, M. J., and Eisenberg, D. (2006) *Proc. Natl. Acad. Sci. U.S.A.* **103,** 4079–4082
52. Kozhukh, G. V., Hagihara, Y., Kawakami, T., Hasegawa, K., Naiki, H., and Goto, Y. (2002) *J. Biol. Chem.* **277,** 1310–1315
53. Hasegawa, K., Ohhashi, Y., Yamaguchi, I., Takahashi, N., Tsutsumi, S., Goto, Y., Gejyo, F., and Naiki, H. (2003) *Biochem. Biophys. Res. Commun.* **304,** 101–106
54. Jones, S., Manning, J., Kad, N. M., and Radford, S. E. (2003) *J. Mol. Biol.* **325,** 249–257